The current issue and full text archive of this journal is available at
www.emeraldinsight.com/0961-5539.htm

Numerical simulation of traveling bubble cavitation

Sunil Mathew, Theo G. Keith Jr and Efstratios Nikolaidis
Mechanical, Industrial and Manufacturing Engineering Department, University of Toledo, Toledo, USA

Received November 2003
Revised March 2005
Accepted June 2005

Abstract

Purpose – The purpose is to present a new approach for studying the phenomenon of traveling bubble cavitation.

Design/methodology/approach – A flow around a rigid, 2D hydrofoil (NACA-0012) with a smooth surface is analyzed computationally. The Rayleigh-Plesset equation is numerically integrated to simulate the growth and collapse of a cavitation bubble moving in a varying pressure field. The analysis is performed for both incompressible and compressible fluid cases. Considering the initial bubble radius as a uniformly distributed random variable, the probability density function of the maximum collapse pressure is determined.

Findings – The significance of the liquid compressibility during bubble collapse is illustrated. Furthermore, it is shown that the initial size of the bubble has a significant effect on the maximum pressure generated during the bubble collapse. The maximum local pressure developed during cavitation bubble collapse is of the order of 10^4 atm.

Research limitations/implications – A single bubble model that does not account for the effect of neighboring bubbles is used in this analysis. A spherical bubble is assumed.

Originality/value – A new approach has been developed to simulate traveling bubble cavitation by interfacing a CFD solver for simulating a flow with a program simulating the growth and collapse of the bubble. Probabilistic analysis of the local pressure due to bubble collapse has been performed.

Keywords Cavitation, Numerical flexibility, Pressure

Paper type Research paper

Nomenclature

c_∞ = velocity of sound in liquid at infinity
k = turbulent kinetic energy
p = pressure
p_∞ = static pressure of undisturbed liquid
p_b = pressure inside the bubble
p_v = vapor pressure of the liquid
p_g = pressure of the non-condensable gas in the bubble
P = static pressure in the liquid
P_c = critical pressure
r = distance from the center of the bubble.
R = bubble radius
R_c = critical radius
R_{max} = maximum bubble radius
R_{min} = minimum bubble radius
$\dot{R}, \ddot{R}$ = first and second derivatives of R with respect to time
t = time
u = fluid velocity
ρ = fluid density
ρ_l = liquid density
ρ_g = gas density
μ = molecular viscosity
μ_t = turbulent viscosity
ε = turbulence dissipation rate
δ_{ij} = kronecker delta
σ = surface tension
ϕ = velocity potential
∇ = gradient operator
γ = specific heat ratio
ζ = liquid bulk viscosity

International Journal of Numerical Methods for Heat & Fluid Flow
Vol. 16 No. 4, 2006
pp. 393-416

0961-5539
DOI 10.1108/09615530610653055

1. Introduction

Traveling bubble cavitation occurs near solid walls when the state of the pressure distribution within the boundary layer is such that neither laminar nor turbulent separation takes place. It is typically encountered on hydrofoils at small incidence angles. The bubbles produced on hydrofoils are generally hemispherical.

Liquids contain nuclei of varying sizes. Each of them is characterized by a critical pressure, P_c. Inception of cavitation is not directly related to the concentration of nuclei but to the critical pressure of the weakest nuclei contained in the liquid (Lecoffre, 1999). The number of bubbles produced depends on the concentration of active nuclei in the liquid. An increase in the concentration of nuclei results in the reduction in the maximum radius attained by the bubbles (Lecoffre, 1999).

An important factor affecting cavitation damage is the generation of extremely high pressures by collapsing bubbles. The growth of a cavitation bubble moving through a varying pressure field is fairly smooth and can be modeled using the Rayleigh-Plesset equation with reasonable accuracy. On the other hand, the collapse process is quite complex. The bubble collapses abruptly and the collapse is followed by successive rebounds and collapses. In the final stages of bubble collapse, the bubble wall velocities reach an appreciable fraction of the speed of sound in the liquid so that the liquid compressibility is no longer negligible (Tomita and Shima, 1977). Liquid compressibility plays an important role in the formation of shock waves during the rebound phase that follows the collapse. The contents of the cavity have a significant effect on the final pressures and on the pressure wave that emanates due to the rebound.

Two characteristic effects are believed to be mainly responsible for the destructive action of cavitation:

(1) the emission of shock waves upon the collapse of the bubble near a solid wall; and

(2) the generation of a high-speed liquid jet directed towards the solid wall.

Apart from the above two, a third effect was pointed out by Shutler and Mesler (1965):

> During the collapse phase, the bubble is attracted towards the boundary, leading to a reduced distance at the moment of collapse. This increases the damage capability of the shock waves.

Hickling and Plesset (1964) were the first to use of numerical solutions of compressible flow equations to explore the formation of pressure waves or shocks as a result of bubble collapse. It was found that the peak pressure attenuates as $1/r$ as it propagates away from the bubble, where r is the distance from the center of the bubble. Recently, based on experimental data, Philipp and Lauterborn (1998) concluded that only bubbles collapsing on the surface caused erosion. When a cavitation bubble collapses near a solid surface, intense disturbances are produced, which generate highly localized and transient surface stresses (Brennen, 1995). Repetition of this loading due to repeated collapses causes local surface fatigue failure and the subsequent detachment of material from the surface.

Cavitation, in most cases, is responsible for undesirable effects, such as, noise, damage to surfaces and loss in performance of hydraulic machinery. Nevertheless, there are also some useful applications. These include ultrasonic machining, ink-jet printing, and ultrasonic dental cleaning (Lecoffre, 1999). In most applications, cavitation acts as an amplifier of flow effects by focusing the local energy. A better

understanding of the physics behind this phenomenon could help in the development of tools for predicting the pressure on a wall induced by cavitation.

In the last decade, significant progress has been achieved in the field of cavitation modeling based on the solution of the Navier-Stokes equations. These studies can be put into two categories. In one category, the cavity region is assumed to have a constant pressure equal to the vapor pressure of the corresponding liquid and the computations are performed only for the liquid phase. The liquid-vapor interface is tracked based on this assumption. In the second category, flows of both phases are computed. A volume fraction equation is solved along with the flow equations to simulate the cavitating flow. These cavitation models can be used to obtain the volume fraction contours and to track liquid-vapor interface. However, they cannot predict the local pressures developed due to cavitation bubble collapse. The models are good tools to simulate sheet cavitation but, may not be able to predict traveling bubble cavitation very accurately. In order to study the mechanism of cavitation erosion in detail, it is essential to develop a tool that could interface the macroscopic level of the flow field and the microscopic level of the cavitation bubble.

The rest of this paper is organized as follows: Section 2 presents an overview of the proposed approach for tracking a cavitation bubble and for computing the pressure induced by the collapse of the bubble on a solid wall; Section 3 presents a model of a cavitation bubble;. Sections 4 and 5 demonstrate an example using the proposed approach.

2. Approach

An outline of the solution approach is shown in Figure 1. The inlet flow conditions and the geometry of the hydrofoil constitute the input. A computational fluid dynamics (CFD) solver is used to determine the flow field. In this study, the Fluent 6.0 code was used as the CFD solver. The final output is the pressure pulse amplitude on the surface of the hydrofoil.

The following steps are involved in the approach:

(1) Use a CFD solver to simulate 2D steady flow around a hydrofoil for a certain set of input conditions (hydrofoil geometry, angle of attack, free stream velocity, free stream pressure and liquid properties). (It is assumed that the gross velocity and pressure fields for the cavitating flow do not differ from those in non-cavitating flow since we are considering incipient cavitation). Obtain the pressure and velocity fields as a function of space.

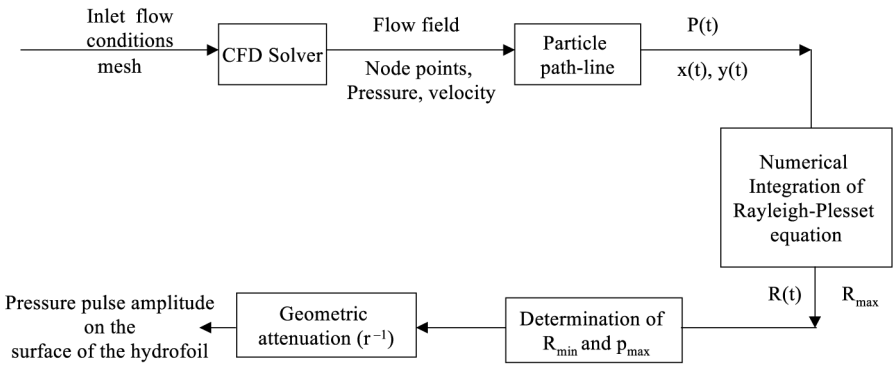

Figure 1.
Block diagram of the solution approach

(2) Determine the pathline of a particle originating at the point corresponding to the minimum pressure coefficient $C_{p\min}$ and moving downstream with the flow. A cavitation bubble originating at the minimum pressure location would travel along the same path. The following procedure can be used to determine the pathline of the bubble:

a) From the results of Step 1. find the node point ($x_{\min}$, $y_{\min}$) corresponding to the minimum pressure location ($C_{p\min}$). This is the position of the pathline of the bubble at time $t = 0$.

b) Find the corresponding velocity vectors $u_x(t = 0)$, $u_y(t = 0)$ and Pressure $P(t = 0)$.

c) Compute the displacement of the bubble Δx, Δy, in time Δt.

d) Find the node point (x_1, y_1) corresponding to the position of the bubble at $t_1 = t + \Delta t$.

e) Find the velocity vectors $\mathbf{u}_x(t = t_1)$, $\mathbf{u}_y(t = t_1)$ and the pressure $P(t_1)$ corresponding to node point (x_1, y_1).

f) Repeat steps c, d and e to determine the position of the bubble as a function of time ($x(t)$, $y(t)$) and the external static pressure acting on the bubble as a function of time, $P(t)$.

(3) Perform numerical integration of the Rayleigh-Plesset equation for a bubble with initial radius, R_0, moving in a varying pressure field given by $P(t)$ and determine the radius of the bubble as a function of time $R(t)$. Find the maximum bubble radius $R_{\max}$.

(4) Evaluate the partial pressure (p_{g_0}) due to non-condensable gas in the bubble corresponding to the initial bubble radius, R_0. Find the gas pressure p_{g_m} corresponding to the maximum radius $R_{\max}$ assuming isothermal expansion. Determine the minimum radius ($R_{\min}$) by numerical integration of the equation of motion of the bubble wall (including liquid compressibility effects), and find the corresponding pressure generated in the bubble.

(5) Find the shortest distance between the bubble center and the hydrofoil surface at the beginning of the collapse. Determine the peak pressure amplitude on the hydrofoil surface due to bubble collapse.

In order to obtain a solution to the problem, the following set of simplifying assumptions were made:

- The cavitation bubble is spherical throughout the growth and collapse.
- The growth and collapse is treated as if there is a single bubble in the liquid field.
- Bubble growth phase is isothermal and collapse phase is adiabatic.
- Partial pressure of the non-condensable gas inside the bubble is negligible in the bubble growth phase.
- The mass of non-condensable gas contained in the bubble is constant.
- Thermal effects are negligible.
- Liquid compressibility and viscosity effects are negligible in the growth phase.

2.1 CFD solver

Fluent 6.0, which is a well known, commercially available, CFD solver, was used to simulate the steady flow around a rigid, 2D hydrofoil (NACA-0012). The pressure field is calculated from the pressure distribution over the hydrofoil in non-cavitating flow. It is assumed that the pressure coefficient is not significantly affected by the cavitation bubbles in the flow. The standard k-ε model with standard wall functions is used to account for the turbulence effects in the flow.

2.1.1 Governing equations: Reynolds-averaged Navier-Stokes (RANS) equations. The flow under consideration is a 2D, incompressible and turbulent flow. The governing equations for 2D incompressible flow are:

$$\frac{\partial \rho}{\partial t} + \frac{\partial}{\partial x_i}(\rho u_i) = 0 \tag{1}$$

$$\rho\left(\frac{\mathrm{d}u_i}{\mathrm{d}t}\right) = -\frac{\partial p}{\partial t} + \frac{\partial}{\partial x_j}\left[\mu\left(\frac{\partial u_i}{\partial x_j} + \frac{\partial u_j}{\partial x_i} - \frac{2}{3}\delta_{ij}\frac{\partial u_i}{\partial x_i}\right)\right] + \frac{\partial}{\partial x_j}\left(-\rho\overline{u_i' u_j'}\right) \tag{2}$$

"Reynolds stresses" $-\rho\overline{u_i' u_j'}$, must be modeled in order to close the system of equations. The Boussinesq hypothesis relates the Reynolds stresses to the mean velocity gradients as:

$$-\rho\overline{u_i' u_j'} = \mu_t\left(\frac{\partial u_i}{\partial x_j} + \frac{\partial u_i}{\partial x_j}\right) - \frac{2}{3}\left(\rho k + \mu_t \frac{\partial u_i}{\partial x_i}\right)\delta_{ij} \tag{3}$$

where μ_t is the turbulent viscosity. The Boussinesq hypothesis is used in the k-ε model. Two additional transport equations (for the turbulent kinetic energy, k and the turbulence dissipation rate, ε) must be introduced and solved.

3. Single bubble model

Consider a spherical bubble with radius R in a liquid with static pressure, P. The pressure inside the bubble is p_b. (Figure 2):

$$p_\mathrm{b} = P + 2\sigma/R \tag{4}$$

$$p_\mathrm{b} = p_\mathrm{g} + p_\mathrm{v} \tag{5}$$

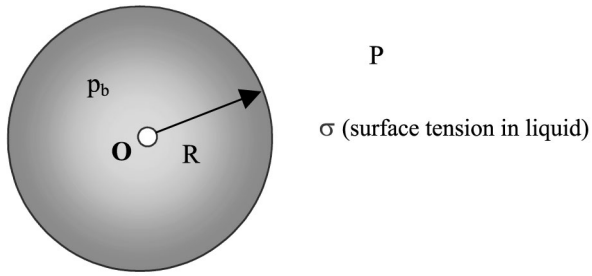

Figure 2.
Spherical bubble in a liquid

The pressure of the gas at constant temperature, p_g, is given by:

$$p_g = \text{constant}/R^3 \tag{6}$$

Corresponding to a particular state of the bubble denoted by subscript "0" we have:

$$p_{g_0} + p_v = P_0 + \frac{2\sigma}{R_0} \tag{7}$$

The equation for the quasi-static isothermal response of a bubble for a radius R is:

$$p_{g_0}\left(\frac{R_0}{R}\right)^3 + p_v = P + \frac{2\sigma}{R} \tag{8}$$

A given bubble is characterized by a critical pressure P_c and a critical radius R_c. At the critical point where the pressure becomes maximum, $dP/dR = 0$. On differentiating the equilibrium equation, equation (5), with respect to R and letting $dP/dR = 0$, we get:

$$R_c = \left(\sqrt{\frac{3}{2}p_{g_0}\frac{R_0}{\sigma}}\right)R_0 \tag{9}$$

Combining equations (8) and (9) produces the following relation between the critical pressure, p_c, and critical radius R_c:

$$P_c - p_v = -\frac{4}{3}\frac{\sigma}{R_c} \tag{10}$$

This expression reveals that the critical pressure is always lower than the vapor pressure of the liquid and can become negative for a sufficiently small value of the critical radius.

3.1 Bubble dynamics: Rayleigh-Plesset equation

Consider a bubble moving through a region in which the pressure varies with time. Let the center of the bubble be the origin "O" and let "M" be any point at a distance r from the origin. $P(t)$ is the static pressure in the liquid at a distance from the bubble and R is the instantaneous radius of the bubble at time t (Figure 3).

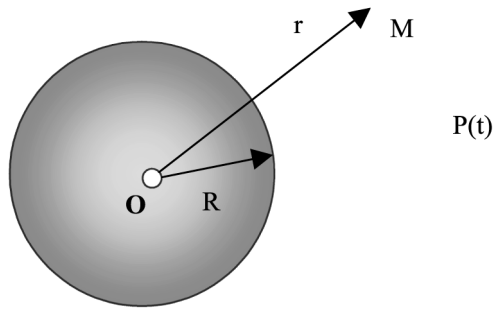

Figure 3.
Spherical bubble in a varying pressure field

The velocity potential ϕ for motion of the liquid with spherical symmetry is:

$$\phi = \frac{R^2\dot{R}}{r} \tag{11}$$

where $\dot{R} = \mathrm{d}R/\mathrm{d}t$.

Bernoullis' equation for an unsteady flow of an irrotational liquid may be written as:

$$-\frac{\partial\phi}{\partial t} + \frac{1}{2}(\nabla\phi)^2 + \frac{p(r)}{\rho_l} = \frac{P(t)}{\rho_l} \tag{12}$$

where $p(r)$ is the static pressure at a distance r.

From equation (11) we have:

$$(\nabla\phi)^2 = \frac{R^4\dot{R}^2}{r^4} \tag{13}$$

and:

$$\frac{\partial\phi}{\partial t} = \frac{1}{r}(2R\dot{R}^2 + R^2\ddot{R}) \tag{14}$$

Substituting equations (13) and (14) in equation (12) and setting $r = R$, the equation of motion for the bubble radius is determined, i.e.:

$$(\nabla\phi)^2|_{r=R} = \dot{R}^2 \tag{15}$$

$$\frac{\partial\phi}{\partial t}|_{r=R} = 2\dot{R}^2 + R\ddot{R} \tag{16}$$

Thus, equation (12) becomes:

$$\frac{p(R) - P(t)}{\rho_l} = \frac{3}{2}\dot{R}^2 + R\ddot{R} \tag{17}$$

Equation (17) is known as the Rayleigh-Plesset equation, which is the general equation of motion for a spherical bubble in a liquid with given external pressure $P(t)$.

From equations (4) and (5) we have:

$$p(R) = p_\mathrm{b} - \frac{2\sigma}{R} = p_\mathrm{v} + p_\mathrm{g} - \frac{2\sigma}{R} \tag{18}$$

Neglecting the pressure due to the non-condensable gas p_g, we have $p_\mathrm{b} = p_\mathrm{v}$ and the Rayleigh-Plesset equation (equation (17)), takes the form:

$$R\ddot{R} + \frac{3}{2}\dot{R}^2 = \frac{p_\mathrm{v} - \frac{2\sigma}{R} - P(t)}{\rho_l} \tag{19}$$

or:

$$R\ddot{R} + \frac{3}{2}\dot{R}^2 = \frac{p_\mathrm{v} - P(t)}{\rho_l} - \frac{2\sigma}{\rho R} \tag{20}$$

The above equation could be solved analytically if the value of $P(t)$ is a constant say, P_0. In that, the equation (20) reduces to the Rayleigh equation. In the case of varying external pressure $P(t)$, numerical integration of the equation (20) is required to obtain a solution. The solution is determined when the two initial conditions are specified.

3.1.1 Effect of viscosity. The equation of motion of a bubble in a viscous liquid is given by the following equation:

$$R\ddot{R} + \frac{3}{2}\dot{R}^2 = \frac{1}{\rho_l}\left(p_v - P - \frac{2\sigma}{R} - 4\mu\frac{\dot{R}}{R}\right) \tag{21}$$

In a liquid such as water, with a small coefficient of viscosity, the viscous term has a negligible effect on a growing bubble. However, during the final stage of collapse, the value of $\dot{R}$ becomes very large and the viscous effects cannot be neglected.

3.1.2 Thermal effects. During the bubble growth, a cooling effect is produced due to evaporation leading to a temperature decrease. Conversely, as the bubble collapses, vapor condensation causes the temperature to rise. The variation in the temperature causes a change in the vapor pressure (p_v) that can significantly affect the bubble dynamics. However, cavitation bubbles in usual hydrodynamic situations occur at temperatures appreciably below the ordinary boiling temperature, so that the vapor density and pressure are small. Under such a condition, the thermal effects may be neglected over the entire growth phase and the nearly all of the collapse phase (Brennen, 1995).

3.2 Determination of pressure generated due to cavitation bubble collapse

The equilibrium equation for a micro-bubble with radius R_0 subjected to external static-pressure, P, are developed from:

$$p_b = P + \frac{2\sigma}{R_0} \tag{22}$$

$$p_{g_0} + p_v = P + \frac{2\sigma}{R_0} \tag{23}$$

$$p_{g_0} = P + \frac{2\sigma}{R_0} - p_v \tag{24}$$

Assuming the bubble growth process is isothermal, we can determine the partial pressure of the gas in the bubble corresponding to maximum bubble radius R_{max} (R_{max} is obtained by numerical integration of the Rayleigh-Plesset equation):

$$p_{g_m} = p_{g_0}\left(\frac{R_0}{R_{max}}\right)^3 \tag{25}$$

The minimum radius attained by the bubble corresponding to the gas pressure, p_{g_m} and a maximum bubble radius R_{max} (Hickling and Plesset, 1964), is given by:

$$R_{\min} = R_{\max}\left[\frac{1}{(\gamma-1)}\frac{p_{g_m}}{\left(P - p_v - p_{g_m} + \frac{3\sigma}{R_{\max}}\right)}\right]^{\frac{1}{3(\gamma-1)}} \tag{26}$$

where P is the static pressure in the liquid and p_v is the vapor pressure of the liquid.

The maximum impulsive pressures $p_{\max}$ occurring during the bubble collapse for incompressible liquid can be estimated as follows (Plesset and Perry, 1962):

$$p_{\max} = p_{g_m}\left(\frac{R_{\max}}{R_{\min}}\right)^{3\gamma} - \frac{2\sigma}{R_{\min}} \tag{27}$$

where, p_{g_m} is the gas pressure inside the bubble at the beginning of the collapse, $R_{\max}$ is the radius of the bubble at the beginning of the collapse, $R_{\min}$ is the minimum bubble radius and γ is the ratio of specific heats for the gas.

3.2.1 Effect of liquid compressibility. As mentioned earlier, the liquid compressibility cannot be neglected while analyzing the bubble collapse process. Moreover, since the bubble collapse occurs in an extremely short period of time, the process can be considered adiabatic and governed by the relation $PV^{\gamma} = \text{constant}$; where, P is the pressure, V is the volume and γ is the specific heat ratio. Tomita and Shima (1977) derived the equation of motion of a spherical bubble in a viscous compressible liquid. The equation of motion of the bubble with first order correction for the liquid compressibility is:

$$R\ddot{R}\left[1 - (1+\varepsilon)\frac{\dot{R}}{c_\infty}\right] + \frac{3}{2}\dot{R}^2\left(\frac{4-\varepsilon}{3} - \frac{4}{3}\frac{\dot{R}}{c_\infty}\right) + \frac{1}{\rho_l}\left(P - p_{r=R} - \frac{R\dot{p}_{r=R}}{c_\infty}\right) = 0 \tag{28}$$

where:

$$\varepsilon = 1 - \frac{\rho_g}{\rho_l} = 0.99881,$$

$$p_{r=R} = p_{g_m}\left(\frac{R_{\max}}{R}\right)^{3\gamma} - \frac{2\sigma}{R} \tag{29}$$

and:

$$\dot{p}_{r=R} = -3\gamma p_{g_m}\frac{\dot{R}}{R}\left(\frac{R_{\max}}{R}\right)^{3\gamma} + \frac{2\sigma}{R^2}\dot{R} \tag{30}$$

In these expressions, p_{g_m} is the non-condensable gas pressure inside the bubble corresponding to the maximum bubble radius.

The maximum impulse pressure corresponding to the minimum bubble radius $R_{\min}$ is given by the following (Tomita and Shima, 1977):

$$p_{\max} = p_{g_m}\left(\frac{R_{\max}}{R_{\min}}\right)^{3\gamma} - \frac{2\sigma}{R_{\min}} + \frac{4\mu\left(\frac{4\mu}{3} + \xi\right)}{\rho_l^2 R_{\min}^2 c_\infty^2}\left(p_{g_m}\left(\frac{R_{\max}}{R_{\min}}\right)^{3\gamma} - \frac{2\sigma}{R_{\min}} - P\right) \tag{31}$$

3.3 Formulation

The Rayleigh-Plesset equation is written as:

$$R\ddot{R} + \frac{3}{2}\dot{R}^2 = \frac{p_v - P(t)}{\rho} - \frac{2\sigma}{\rho R} \tag{32}$$

where $\dot{R} = dR/dt$ and $\ddot{R} = d^2R/dt^2$.

Rearranging terms we get:

$$\ddot{R} = \frac{1}{\rho R}[p_v - P(t)] - \frac{3}{2R}(\dot{R})^2 - \frac{2\sigma}{\rho R^2} \tag{33}$$

To numerically solve this ordinary differential equation, the Runge-Kutta method (Kellison, 1975; Hornbeck, 1975; Maron, 1987) is used. To accomplish this, equation (33) is written as two first-order differential equations:

$$f_1(t, z, R) = z' = \frac{1}{\rho R}[p_v - P(t)] - \frac{3}{2R}(z)^2 - \frac{2\sigma}{\rho R^2} \quad |z(0) = 0 \tag{34}$$

$$f_2(t, z, R) = R' = z \quad |R(0) = R_0 \tag{35}$$

The two equations have to be solved simultaneously. Since, the equation is non-linear, the coefficients in the expression for f_1 are unknown at each step. This problem can be solved by taking a suitably small time step (Δt) and using the value of R from the previous time step. The value of $P(t)$ is taken from the array of pressure values that gives the external pressure acting on the bubble as a function of time.

4. Validation

4.1 Validation of the Fluent solver using airfoil data

The Fluent solver was used to simulate the steady flow of air around an airfoil (NACA-0012) to compute the section lift and drag coefficients. The results were compared to experimental data for a NACA-0012 wing section (Abbott and Doenhoff, 1987). Figure 4 shows the variation in the section lift coefficient as the angle of attack of the airfoil is varied from 0° to 8°. As may be seen, the relationship between angle of attack and the section lift coefficient is almost linear. The solver output coincides with the experimental results. Figure 5 shows the relation between the section lift and drag coefficients.

It can be observed that the solver is able to reproduce the experimental results accurately, particularly for lower angles of attack. However, there is a slight deviation that is observed as the angle of attack is increased.

4.2 Validation of the numerical simulation of the bubble growth

Plesset (1949) used numerical integration of the Rayleigh-Plesset equation to simulate the growth and collapse of a cavitation bubble moving in a varying pressure field.

The results obtained by Plesset were used to validate the computer code used in this study to numerically simulate cavitation bubble dynamics. The varying pressure field, $P(t)$, obtained from the experimental data (Plesset, 1949) is inputted into the program to predict the growth and collapse of the cavitation bubble. The integration constants of the equation of motion were fixed by using the experimentally observed value for the maximum radius R_{max}, where $\dot{R} = 0$. The bubble dynamics is simulated by integrating backward (growth portion) and forward (collapse portion) from the point corresponding to the maximum radius, R_{max}.

The bubble dynamics curve for given pressure function $P(t)$ is shown in Figures 6 and 7. The output of the program agrees quite well with the results obtained by Plesset (1949).

4.3 Validation of the method used to determine the bubble collapse pressure

As mentioned, liquid compressibility effects have to be accounted for in the bubble collapse analysis. The equation of motion for the bubble wall derived by Tomita and Shima (1977) has been applied to simulate the bubble collapse. The fourth-order Runge-Kutta method is used for the numerical integration of equation (25). The bubble collapses from a maximum radius R_{max} to a minimum radius R_{min}. The maximum collapse pressure p_{max} is determined using equation (31). The pressure of the gas inside

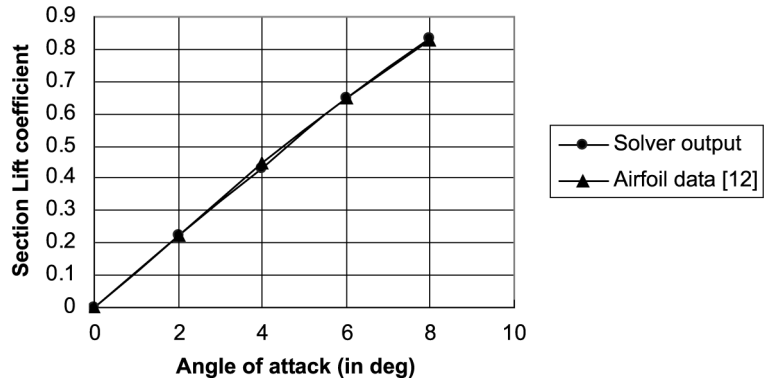

Figure 4.
Comparison of solver results with airfoil data for NACA-0012 wing section (Chord Reynolds number 4.5×10^6)

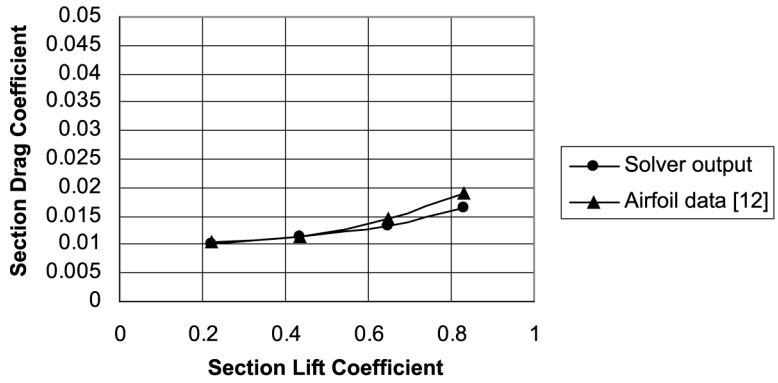

Figure 5.
Comparison of solver results with airfoil data for NACA-0012 wing section: drag vs lift coefficient (Chord Reynolds number 4.5×10^6)

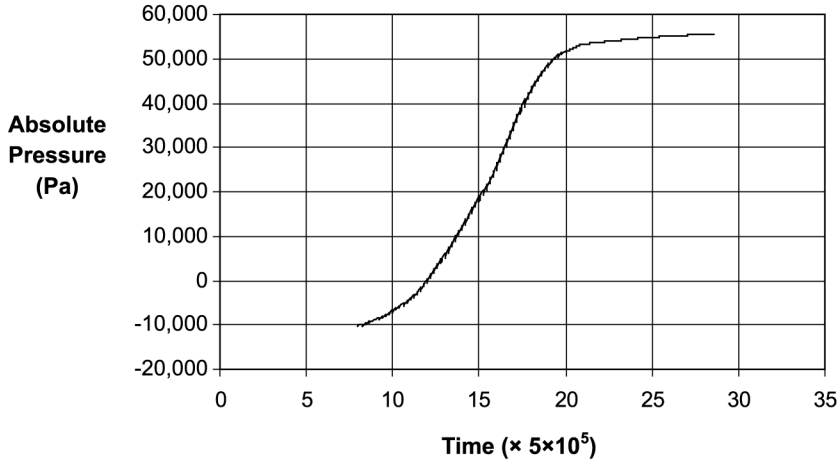

Figure 6.
External pressure $P(t)$ acting on the cavitation bubble as a function of time

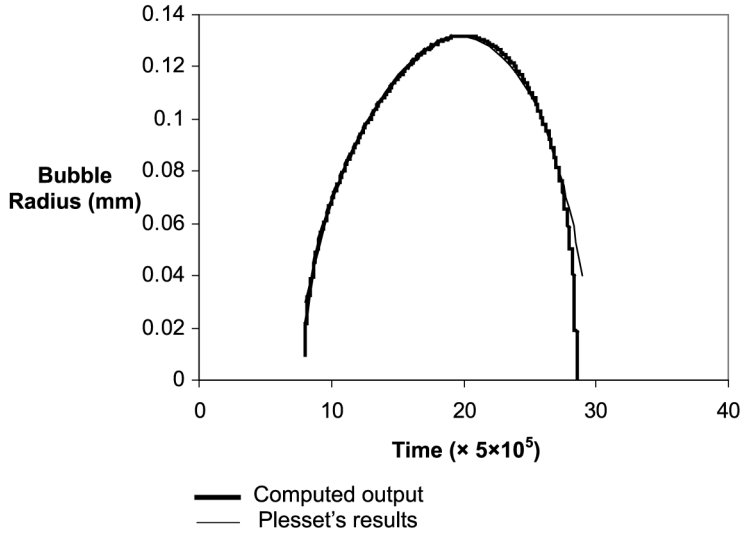

Figure 7.
Bubble dynamics $R(t)$. Comparison between the FORTRAN output and the results obtained by Plesset (1949)

the bubble, p_g, has a significant effect on the collapse pressure. The results obtained by Tomita and Shima (1977) were used to validate the method for determining the bubble collapse pressure. A comparison between the results obtained by Tomita and Shima and the computed results is shown in Table I. The minimum bubble radius R_{min} and the maximum collapse pressure p_{max} have been calculated for different combinations of the bubble radius R_{max} and the gas pressure p_g.

The results are comparable for higher values of p_g. As the gas pressure is reduced, there is a significant increase in the magnitude of the collapse pressure and a deviation

p_g(Pa)	R_{max}	10 mm		1 mm		0.1 mm		0.01 mm	
		R_{min} (m)	P_{max} (atm)	R_{min} (m)	P_{max} (atm)	R_{min} (m)	P_{max} (atm)	R_{min} (m)	P_{max} (atm)
10,130	(Tomita and Shima, 1977)	2.73E − 03	23	2.72E − 03	23	2.70E − 03	24	2.51E − 03	33
	Computed value	2.72E − 03	23	2.72E − 03	23	2.69E − 03	24	2.41E − 03	38
5,065	(Tomita and Shima, 1977)	1.71E − 03	83	1.71E − 03	83	1.69E − 03	86	1.58E − 03	113
	Computed value	1.71E − 03	83	1.70E − 03	84	1.68E − 03	88	1.50E − 03	140
2,026	(Tomita and Shima, 1977)	9.23E − 04	444	9.22E − 04	445	9.17E − 04	456	8.73E − 04	559
	Computed value	9.15E − 04	459	9.14E − 04	462	9.03E − 04	485	8.16E − 04	742
1,013	(Tomita and Shima, 1977)	5.98E − 04	1,373	5.97E − 04	1,376	5.95E − 04	1,399	5.74E − 04	1,620
	Computed value	5.86E − 04	1,495	5.85E − 04	1,501	5.79E − 04	1,568	5.38E − 04	2,138

Table I.
Comparison of the computed values with the results of Tomita and Shima (1977)

in the results is observed. Figure 8 shows the dynamics of a collapsing bubble for two different values of the gas pressure p_g. The computational code was able to reproduce the results obtained by Tomita and Shima (1977).

It is observed that the bubble collapse is followed by a series of rebounds. The maximum radius attained by the bubble in the rebound progressively decreases. It can be seen that the gas pressure inside the bubble has a significant effect on the bubble dynamics.

5. Numerical simulation

5.1 Problem description

The approach developed in this study is applied to the following problem: steady turbulent flow around a stationary, rigid 2D hydrofoil (NACA-0012). The geometric and ambient conditions are shown in Table II and the fluid properties are presented in Table III.

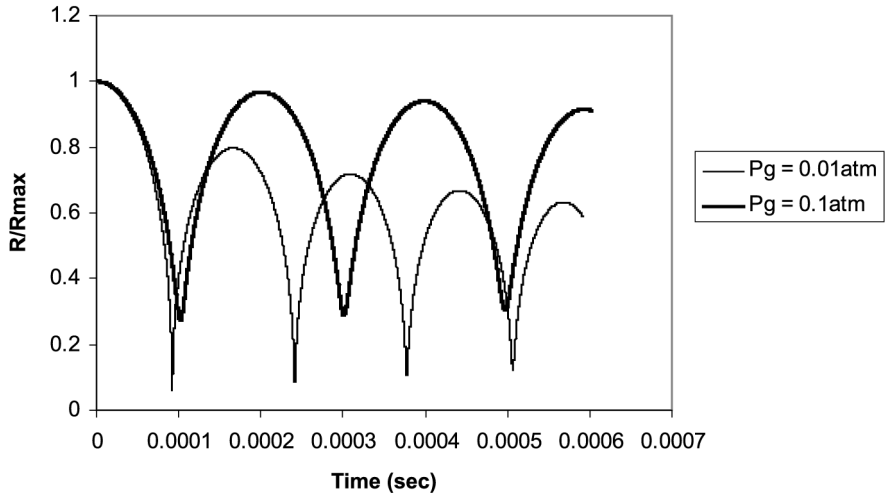

Figure 8.
Collapsing bubble dynamics: initial bubble radius = 1 mm

Table II. Problem specifications	Chord length	10 cm
	Angle of attack	0°
	Inlet flow	25 m/s
	Free stream pressure	1 atm (101,300 Pa)

Table III. Fluid properties at 20°C	Density of water	998.32 kg/m^3
	Viscosity of water	1.003×10^{-3} Ns/m^2
	Bulk viscosity of water	4.7×10^{-3} Ns/m^2
	Surface tension of water	7.247×10^{-2} N/m
	Density of dry air	1.1668 kg/m^3

5.2 Results

Based on the approach outlined above, the simulation of traveling bubble cavitation was performed. The Fluent solver was used to determine the flow field for flow around a rigid 2D hydrofoil. The flow is turbulent, 2D unsteady. The standard k-ε turbulence model was used with a 2 percent inlet turbulence intensity. The information obtained from the solver output was incorporated into the bubble dynamics simulation code to simulate the growth and collapse of a cavitation bubble moving along the surface of the hydrofoil. Figure 9 shows the mesh used for the simulation.

An enlarged view of the mesh showing the hydrofoil is shown in Figure 10. It can be observed that the node density is high near the hydrofoil, especially near the leading and trailing edges. This is necessary since the gradients are very high in this region of the flow field.

5.2.1 Results from Fluent solver. The following are the results obtained from the Fluent solver used to determine the velocity and pressure fields.

5.2.1.1 Pressure contours. Figure 11 shows the pressure contours in the flow field. Since, the angle of attack is zero the pressure distribution is symmetrical about the hydrofoil centerline.

5.2.1.2 Velocity distribution. Figure 12 shows the velocity vectors in the flow around the hydrofoil. It can be seen that the flow is streamlined and the maximum velocity zone corresponds to the minimum pressure zone in Figure 11.

5.2.1.3 Pressure distribution along the hydrofoil surface. Figure 13 shows the distribution of static pressure along the surface of the hydrofoil. The leading edge of

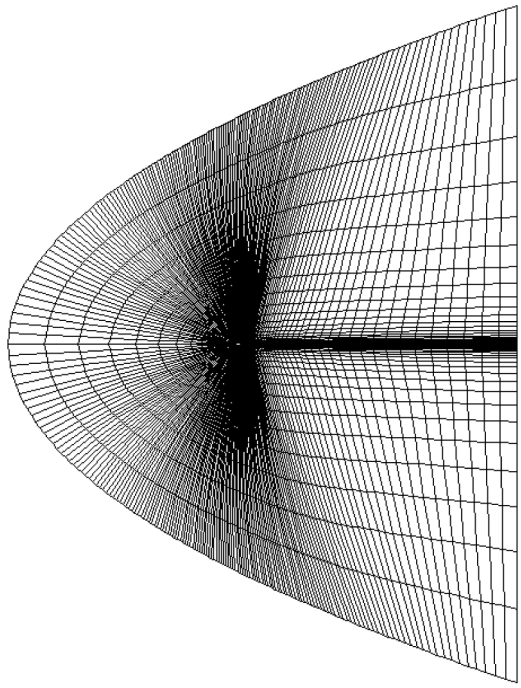

Figure 9.
Mesh

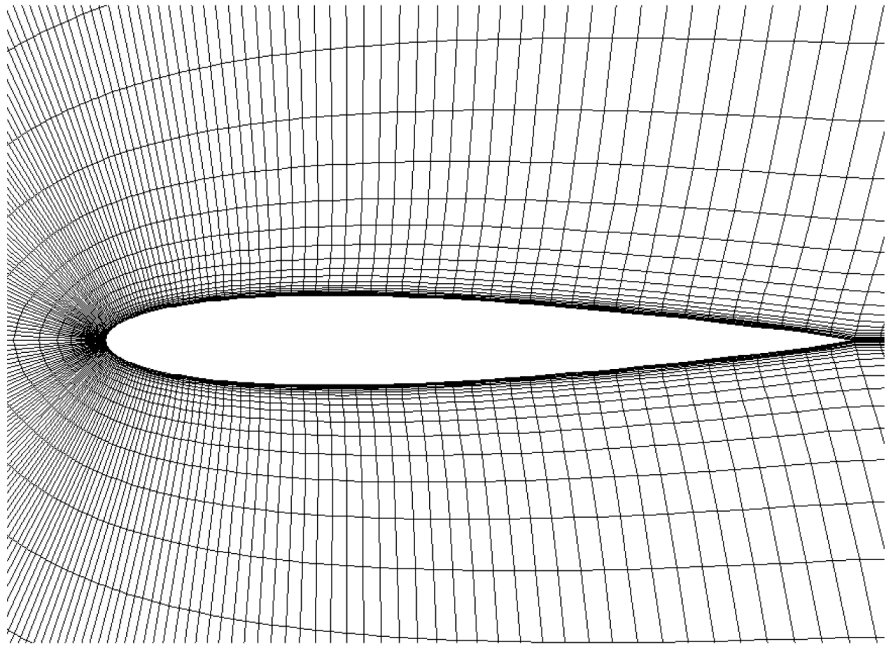

Figure 10.
Enlarged view of the mesh showing the hydrofoil

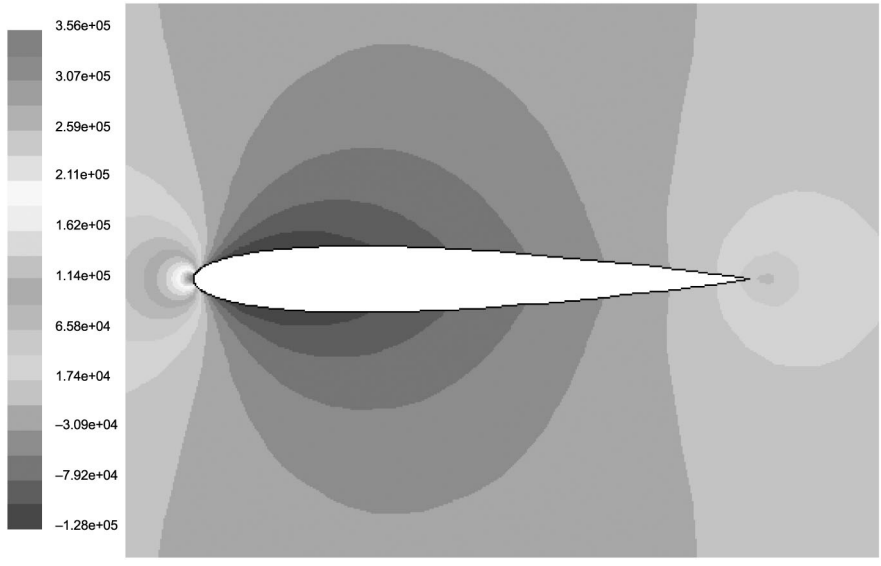

Figure 11.
Static pressure contours around the hydorfoil (showing gauge pressure in Pa)

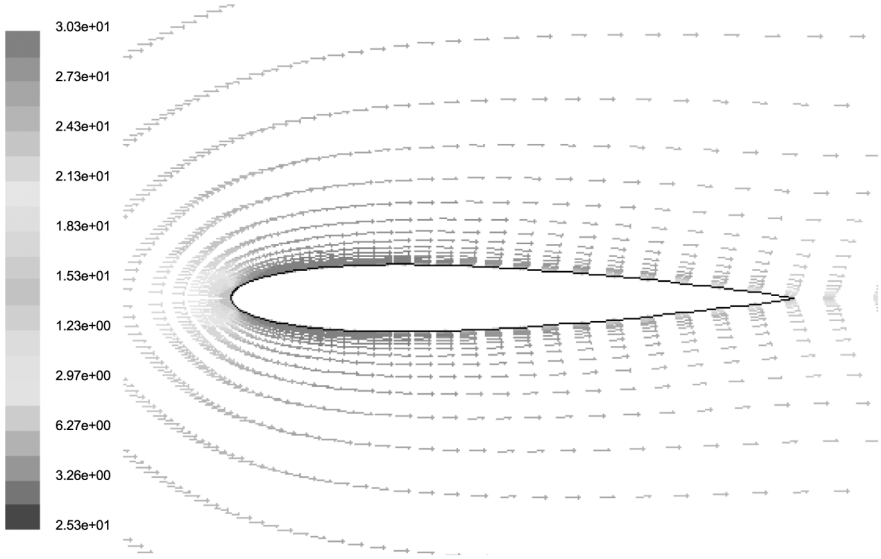

Figure 12.
Velocity vectors around the hydrofoil (colored by velocity magnitude in m/s)

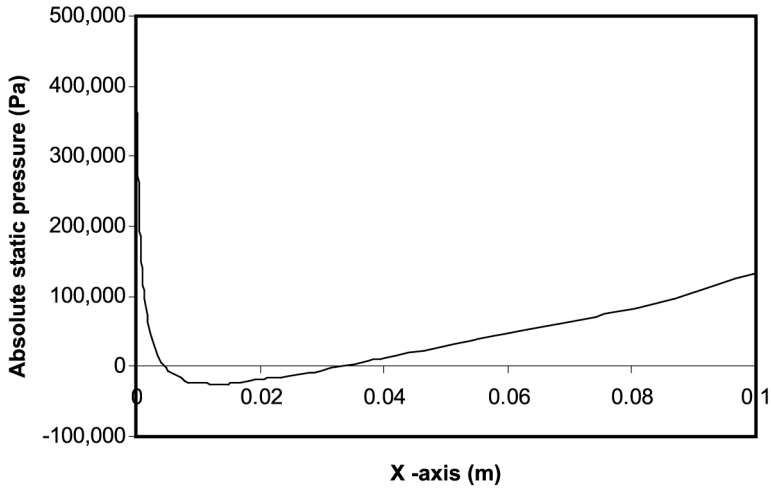

Figure 13.
Static pressure distribution along the hydrofoil surface

the hydrofoil experiences very high pressure. The static pressure drops rapidly as we move along the surface corresponding to increasing flow velocity. After the minimum pressure point, the static pressure begins to rise.

5.2.2 Simulation of the bubble growth and collapse. The results of the solver are used as input for the method that numerically simulates the growth and collapse of a cavitation bubble. The input data consists of the following:

- Co-ordinates (x,y) of all the nodes in the flow field.
- Static pressure, $P(x,y)$.

- Velocity components, $\mathbf{u}_x$ and $\mathbf{u}_y$.
- Derivatives of the velocity with respect to x and y.
- Initial conditions: $R(0) = R_0$ and $\dot{R}(0) = 0$.

It is important to select an appropriate time step size, Δt, to ensure the accuracy of the results. This can be accomplished by performing a parametric study for the time step size. The numerical simulation of the bubble growth is performed for various values of Δt and the corresponding maximum bubble radius, R_{max}, is determined. Figure 14 shows the results of the parametric study.

It can be observed that the value of the maximum bubble radius R_{max} converges as the time-step size is decreased. A time-step size of 10^{-7} s is considered as an optimum value for the problem at hand.

Table IV shows the results of the example to illustrate the method for the simulation of the bubble growth and collapse. The initial bubble radius, R_0, was assumed equal to 100 μm.

Figure 15 shows the variation in the bubble radius as the cavitation bubble moves along the surface of the hydrofoil. The bubble begins to grow as it passes the minimum pressure zone where, the absolute static pressure is $-26{,}100.00$ Pa. The external pressure, $P(t)$, gradually increases as the bubble travels along the surface of the

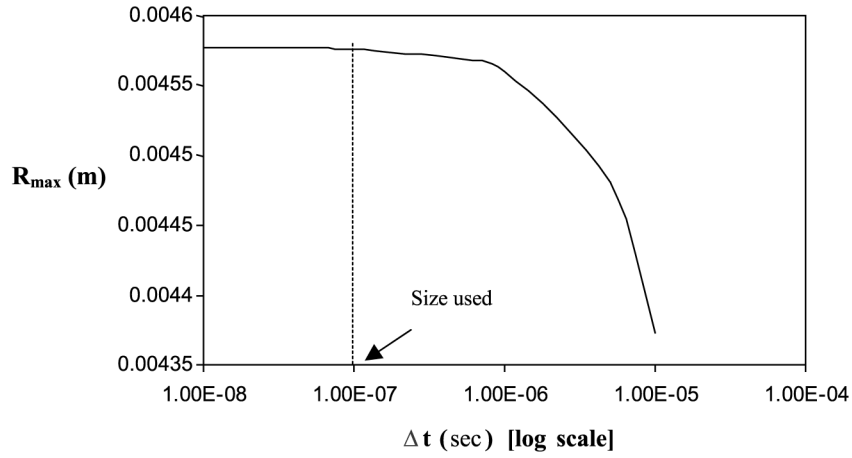

Figure 14.
Time step size

1	Maximum bubble radius (R_{max})	m	4.61×10^{-3}
2	Distance between wall and bubble center during collapse (L)	m	3.344×10^{-4}
3	Initial gas pressure inside the bubble (p_{g_0})	Pa	100,438.00
4	Gas pressure inside the bubble corresponding to the maximum radius (p_{g_m})	Pa	1.024
5	Minimum bubble radius (R_{min})	m	1.35×10^{-5}
6	Maximum pressure generated due to collapse (p_{max})	atm	441,666.00
7	Peak pressure on the hydrofoil surface (p_{wall})	atm	17,832.00

Table IV.
Results for $R_0 = 100\ \mu$m

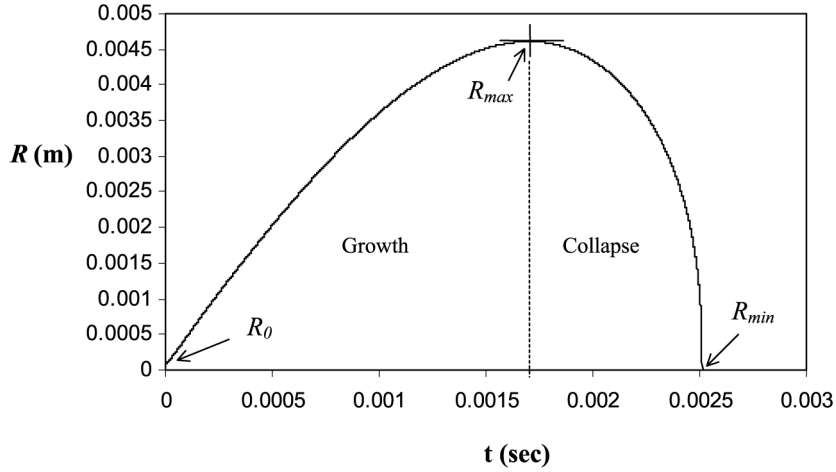

Figure 15.
Variation in the bubble size as a function of time ($R_0 = 100\,\mu$m)

hydrofoil. The cavitation bubble grows from an initial radius, R_0, to a maximum size, R_{max}.

As the bubble grows in size, the partial pressure of the non-condensable gas inside the bubble becomes negligibly small when compared to the vapor pressure. When the external pressure, $P(t)$, exceeds the vapor pressure, the vapor inside the bubble begins to condense into liquid. This results in the collapse of the bubble. The bubble collapses rapidly to a minimum size corresponding to R_{min}. Since, the bubble collapse occurs within an extremely short period, it is assumed that the compression of gas inside the bubble is adiabatic. The collapse of the bubble leads to the generation of very high pressures causing a rebound of the bubble. A pressure pulse is emitted that propagates radially from the bubble center and impinges on the surface of the hydrofoil. The peak amplitude of this pressure pulse attenuates geometrically with distance from the bubble center.

5.2.3 Effect of the initial bubble radius on the maximum collapse pressure. The size of nuclei present in a typical sample of water randomly varies in the range 50-500 μm (Hickling and Plesset, 1964). A parametric study was performed to investigate the effect of the initial bubble radius on the maximum pressure generated during collapse. The results were obtained for both compressible and incompressible fluids. Figure 16 compares the results obtained from compressible and incompressible fluid analysis. The relation between the initial bubble radius, R_0, and the gas pressure in the bubble at the beginning of collapse, p_{g_R}, is shown in Figure 17.

It is clear that the effect of liquid compressibility has greater significance for lower values of R_0, corresponding to lower gas pressures inside the bubble. The results from the compressible and incompressible analyses converge for higher values of the initial bubble radius R_0.

5.3 Probability density function of the maximum collapse pressure

The initial value of the bubble radius, R_0, is uncertain. Assuming a probability density function for this radius, we can determine the probability density function of the maximum pressure due to the collapse of the bubble. When very little information is

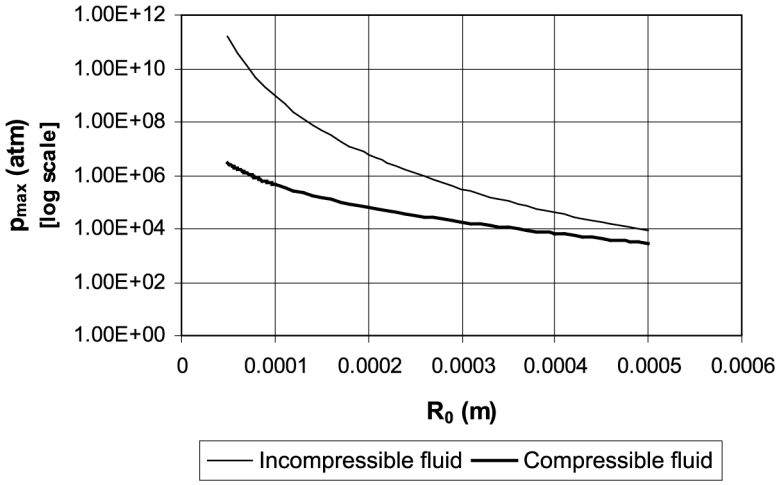

Figure 16.
Effect of the initial bubble size on p_{max}

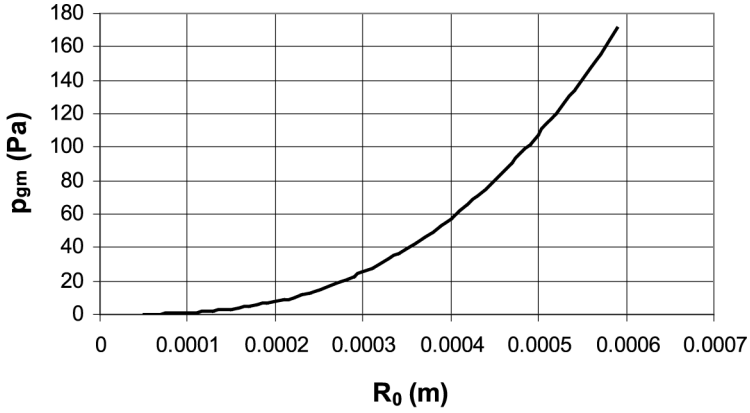

Figure 17.
Relation between R_0 and p_{g_m}

available about a random variable, it is standard practice to obtain lower and upper bounds about the variable based on judgment and to assume a uniform probability density for this variable. The selection of the uniform probability density is motivated by the fact that this distribution has the maximum Shannon's entropy among all distributions that are bounded by the lower and upper limits. It was assumed that the initial radius was uniformly distributed in the range 50-500 μm.

Two approaches can be used to determine the probability density function of the maximum collapse pressure:

(1) a Monte Carlo simulation; and

(2) analytical methods based on probability calculus for the transformation of the random variables.

5.3.1 Monte Carlo simulation. In this approach, N random values of the initial radius in the range 50-500 μm are generated by sampling from a uniform distribution. For each value of the initial bubble radius, the numerical simulation of bubble dynamics is performed and the maximum collapse pressure, $p_{\max}$, is determined. Since, the maximum pressure varies from 10^3 to 10^6 atm, it is convenient to use $\ln(p_{\max})$ for the analysis. The results are displayed in the form of a histogram. The accuracy of increases with the number of simulations (N); the larger the value of N, the greater the accuracy. This approach is simple but can be computationally expensive.

5.3.2 Analytical method. This approach is based on probability calculus for the transformation of random variables. Say, y is a function of a random variable x, that is, $y = g(x)$. Here, x is the independent variable and y is the dependent variable. Given the probability density function of $x : f_X(x)$, the probability density function of $y : f_Y(y)$ can be determined from:

$$f_Y(y) = \frac{f_X(x)}{\frac{dg}{dx}}\Big|_{x=g-1(y)} \tag{36}$$

It is easier to use the analytical method if an expression approximating the maximum pressure as a function of the initial bubble radius is available. Stepwise regression was done to fit a polynomial to approximate the relationship between R_0 and $p_{\max}$.

The data for the regression analysis is obtained by performing the numerical simulation of bubble dynamics for various values of the initial radius (R_0 varying between 50 and 500 μm) and determining the corresponding maximum pressure $p_{\max}$ and $\ln(p_{\max})$. Ninety data points were used for the regression analysis, of which 50 points lie in the range: $50\ \mu\text{m} \leq R_0 \leq 500\ \mu\text{m}$, since there is a large variation in the maximum pressure in this range. A forward stepwise regression method was used for the regression analysis. Since, the magnitude of the R_0 is very small, the values are normalized using the maximum value of the initial radius. The following equation was determined using regression analysis:

$$\ln(p_{\max}) = 16.8076 - 23.5612\left(\frac{R_0}{0.0005}\right) + 27.47\left(\frac{R_0}{0.0005}\right)^2 - 12.9589\left(\frac{R_0}{0.0005}\right)^3 \tag{37}$$

The quality of the approximation obtained from the regression equation can be assessed by the coefficient of determination (Varnderman, 1994). This quantity can be interpreted as the fraction of raw variation in the quantity that is approximately accounted by using approximation (37). The value of the coefficient of determination is 98.8 percent, which suggests an accurate approximation.

Assuming that R_0 is a random variable distributed uniformly in the range 50-500 μm, the probability density function for $\ln(p_{\max})$ could be estimated.

Figure 18 shows the probability density function of the maximum pressure. From this figure, we observe that the most likely values of $\ln(p_{\max})$ are in the range 8-10. This corresponds to $p_{\max}$ falling within the range 3.0×10^3-1.6×10^5 atm. The peak in the graph corresponds to a value of 9.3 for $\ln(p_{\max})$ or $p_{\max} = 1.09 \times 10^4$ atm.

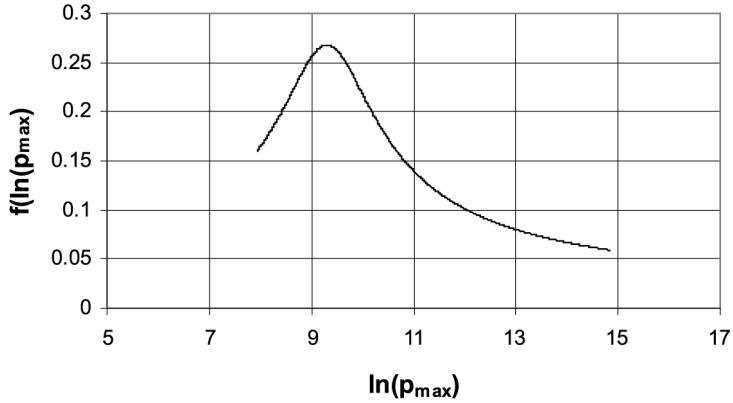

Figure 18.
Probability density function of $\ln(p_{max})$

These results were verified using Monte Carlo simulation with 2,000 randomly generated values for R_0. The results of the Monte Carlo simulation are shown in Figure 19.

The probability density function of $\ln(p_{max})$ can be estimated from the Monte Carlo simulation by dividing the frequency corresponding to each bin value for $\ln(p_{max})$ by the total number of simulations. Figure 20 compares the results obtained analytically and those from Monte Carlo simulation.

As may be seen, the two results agree reasonably well. The small deviation can be explained by the fact that the results obtained from the Monte Carlo simulation are average values of the probability density over the range corresponding to each bin.

5.4 Discussion

The approach used in this paper is based on the assumption that the cavitation bubble is spherical throughout its growth and collapse. However, it is a known fact that the presence of a solid boundary near the cavitation bubble perturbs the spherical symmetry (Benjamin and Ellis, 1966). The adjacent solid boundary has a damping effect on the collapse rate. It is expected that the pressure pulse emitted during collapse is weaker due to bubble deformation. Nevertheless, experimental measurements with

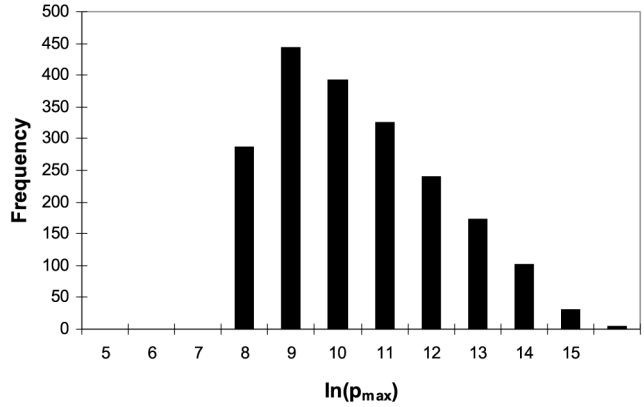

Figure 19.
Monte Carlo simulation results

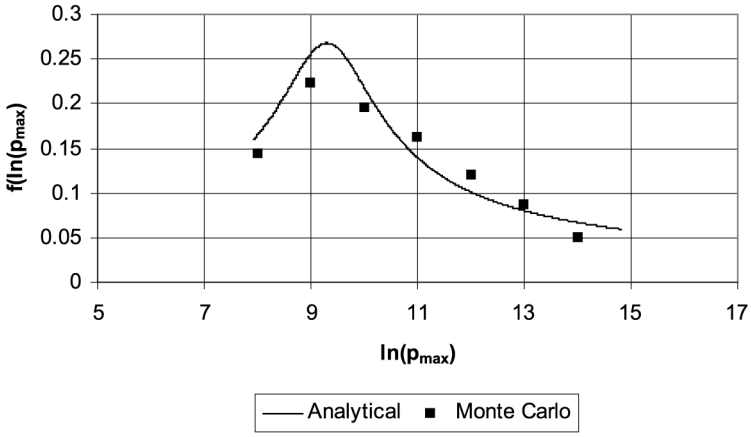

Figure 20.
Comparison between the analytical and Monte Carlo results

single bubbles have confirmed that even in the case of a bubble in contact with the solid boundary, the collapse is accompanied by the emission of shock waves whose pressure amplitudes were as high as 10^4 atm (Lauterborn and Bolle, 1975), which is in agreement with the results obtained herein.

The single bubble model used in this analysis does not account for the effect of neighboring bubbles. The presence of a neighboring bubble has a similar effect as that of a solid boundary. It deforms the spherical symmetry of the bubble resulting in weaker pressure amplitudes during collapse.

6. Conclusions

The major conclusions of this study are:

- A new approach has been developed to simulate traveling bubble cavitation by interfacing a CFD solver for simulating a flow with a program simulating the growth and collapse of the bubble.
- The amount of non-condensable gas (air) inside the cavitation bubble depends on the initial bubble (micronucleus) size, R_0. The initial radius of the cavitation bubble has a significant effect on the maximum pressure generated during collapse.
- The maximum local pressure developed during cavitation bubble collapse is on the order of 10^4 atm.
- Liquid compressibility plays an important role during bubble collapse. The effect of liquid compressibility is significant when the initial bubble radius is very small ($50\,\mu\text{m} \leq R_0 \leq 100\,\mu\text{m}$). For higher values of R_0, the results obtained from compressible and incompressible analyses converge.
- Assuming that the initial bubble radius ($50\,\mu\text{m} \leq R_0 \leq 500\,\mu\text{m}$) is distributed uniformly, the maximum collapse pressure lies in the range 3×10^3 atm-2.8×10^6 atm. The most probable value for the maximum collapse pressure is about 10^4 atm.

References

Abbott, I.H. and Doenhoff, A.E. (1987), *Theory of Wing Sections*, Dover Publications Inc., New York, NY.

Brennen, C.E. (1995), "Cavitation and Bubble Dynamics", Oxford Engineering Science Series 44, Oxford University Press, London.

Benjamin, T.B. and Ellis, A.T. (1966), "The collapse of cavitation bubbles and the pressure thereby produced against solid boundaries", *Phil. Trans. R. Soc. Lond. A*, Vol. 260, pp. 221-40.

Hickling, R. and Plesset, M.S. (1964), "Collapse and rebound of a spherical bubble in water", *The Physics of Fluids*, Vol. 7, pp. 7-14.

Hornbeck, R.W. (1975), *Numerical Methods*, Prentice-Hall Inc., Englewood Cliffs, NJ.

Kellison, S.G. (1975), *Fundamentals of Numerical Analysis*, Richard D Irwin Inc., Homewood, IL.

Lauterborn, W. and Bolle, H. (1975), "Experimental investigation of the cavitation-bubble collapse in the neighborhood of a solid boundary", *Journal of Fluid Mechanics*, Vol. 72, pp. 391-9.

Lecoffre, Y. (1999), *Cavitation Bubble Trackers*, A.A. Balkema Publishers, Brookfield.

Maron, M.J. (1987), *Numerical Analysis: A Practical Approach*, 2nd ed., Macmillan Publishing Company, New York, NY.

Philipp, A. and Lauterborn, W. (1998), "Cavitation erosion by single laser-produced bubbles", *Journal of Fluid Mechanics*, Vol. 361, pp. 75-116.

Plesset, M.S. (1949), "The dynamics of cavitation bubbles", *Journal of Applied Mechanics*, Vol. 16, pp. 277-82.

Plesset, M.S. and Perry, B. (1962), "Cavitation", in Flugge, W. (Ed.), *Handbook of Engineering Mechanics*, McGraw-Hill, New York, NY, pp. 87.1-87.12.

Shutler, N.D. and Mesler, R.B. (1965), "A photographic study of the dynamics and damage capabilities of bubbles collapsing near solid boundaries", *Trans. ASME D: Journal of Basic Engineering*, Vol. 87, pp. 511-7.

Tomita, Y. and Shima, A. (1977), "On the behavior of a spherical bubble and the impulse pressure in a viscous compressible liquid", *Bulletin of the JSME*, Vol. 20, pp. 1453-60.

Varnderman, S.B. (1994), *Statistics for Engineering Problem Solving*, PWS Publishing Company, Boston, MA, p. 107.

Further reading

Li, S.C. (2000), *Cavitation of Hydraulic Machinery*, Imperial College Press, London.

Corresponding author

Theo G. Keith Jr can be contacted at: theo.g.keith@nasa.gov